NEWSLETTER OF THE INTERNATIONAL LIQUID CRYSTAL SOCIETY

Liquid Crystals TODAY

Volume 8, No. 4, December 1998

ISSN: 1358-314X

Smectic Liquid Crystals as Model Systems of Low-dimensional Order

From conformal and independent fluctuations in freely suspended films to true long-range order in smectic elastomers

Wim H. de Jeu, Elisabeth A. L. Mol and Gerard C. L. Wong

FOM-Institute for Atomic and Molecular Physics, Amsterdam, The Netherlands

In this paper we discuss the absence of true long-range order (Landau-Peierls instability) in smectic liquid crystals, which is a direct consequence of the strong thermal fluctuations associated with ordering in less than three dimensions. While the resultant X-ray lineshape has been confirmed already quite some time ago, recently some new aspects have been discovered. In the first place, thanks to modern synchrotron sources, the spectral dependence of the fluctuations in freely suspended smectic films has been determined down to molecular dimensions. While at long wavelengths top and bottom of a film fluctuate in unison, at shorter wavelengths a cross-over to independent fluctuations could be observed. Secondly, in smectic elastomers the stability of the layered structure against fluctuations is dramatically enhanced by the crosslinked architecture. As a result the usual Landau-Peierls instability is no longer observed. Hence we have found the first evidence for existence of long range translational order in soft '1-D' layered systems embedded in 3-D space.

Fluctuations in less than 3-D

Long range translational order is a defining quality of 3-D crystals; it leads to the existence of Bragg reflections. On the other hand, it is a fundamental property of low-dimensional systems (2-D and 1-D) that such a translational periodicity is destroyed by thermal fluctuations [1]. However, we do not need a low-dimensional world to observe such effects; similar arguments apply in 3-D to smectic liquid crystals. As is well known these consist of stacks of fluid monolayers, where rod-like molecules order into a density wave along one direction, but remain fluid in the other two (figure 1(a)).

In such a system the '1-D' translational order of the fluid layers is not truly long-range but decays algebraically with relative position as $r^{-\eta}$ (see figure 2, η small positive). Analogously to 'real' low-dimensional systems, this is due to the thermally induced fluctuations of the smectic layers which can be of two different types.

- Bending of the liquid layers (stiffness constant $K \cong 10^{-11}$ N), during which the layer spacing is maintained.
- Compression and dilatation of the layers (constant $B \cong 10^{6}$ N m^{-2}).

The energetics of these two effects can be expressed in terms of $u(\mathbf{r})$, the layer displacement from its equilibrium position, leading to the Landau-De Gennes free energy density:

$$f = \tfrac{1}{2}B\left(\frac{\partial u}{\partial z}\right)^2 + \tfrac{1}{2}K\left(\frac{\partial^2 u}{\partial x^2} + \frac{\partial^2 u}{\partial y^2}\right)^2.$$

Expanding $u(\mathbf{r})$ in a Fourier series leads to an expression for the free energy density in terms of the modes of the wave vector $\mathbf{k}$ associated with each

(continued on page 2)

In this issue:

Fourier component. Next the equipartition theorem can be used to assign an energy $\frac{1}{2}k_BT$ to each mode. Integrating over all modes leads to the expression for the mean-squared layer displacements:

$$\langle u^2(\mathbf{r})\rangle = \frac{k_BT}{8\pi(BK)^{1/2}} \ln\left(\frac{L}{d}\right) = \eta \ln\left(\frac{L}{d}\right).$$

Here L is the sample size and d the smectic layer spacing. Hence $\langle u^2(\mathbf{r})\rangle$ diverges logarithmically with the sample size; introducing the number of layers $N=L/d$ this divergence takes the form $\ln(N)$.

The effects of the mean squared layer displacement diverging logarithmically with the system size (Landau–Peierls instability) are rather subtle. The resultant X-ray diffraction signature has been calculated by Caillé [2]. In the z-direction perpendicular to the layers, the divergent thermal fluctuations transform the discrete Bragg peaks into algebraic 'cusps' (see figure 2) with the asymptotic power-law form:

$$S(0,0,q_z) \propto \frac{1}{|q_z - q_0|^{2-\eta}},$$

where q is the wave vector transfer (see Appendix figure A1) and $q_0 = 2\pi/d$ represents the position of the first-order diffraction peak. As we see the exponent η of the algebraic decay is directly related to the elastic constants of the system. The magnitude of η is quite small, with typical measured values of $\eta \approx 0.1–0.3$ near the smectic-A/nematic

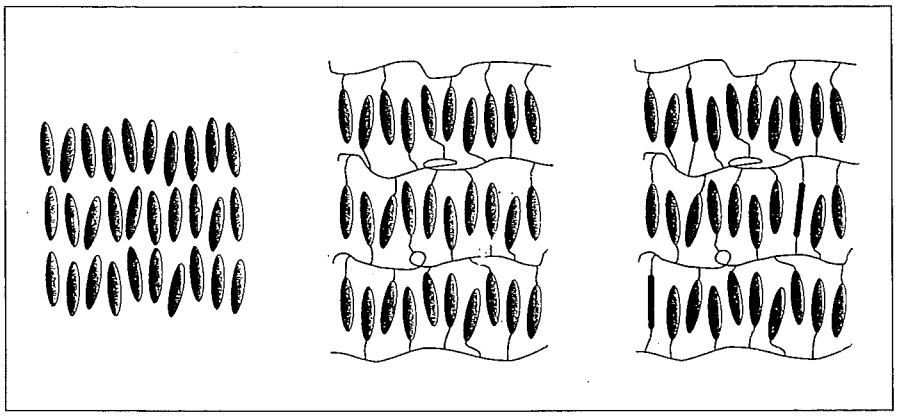

Figure 1. Schematic representation of (*a*) a smectic liquid crystal, (*b*) a smectic liquid crystalline polymer and (*c*) a weakly crosslinked smectic elastomer network. Crosslinks are represented by cylinders.

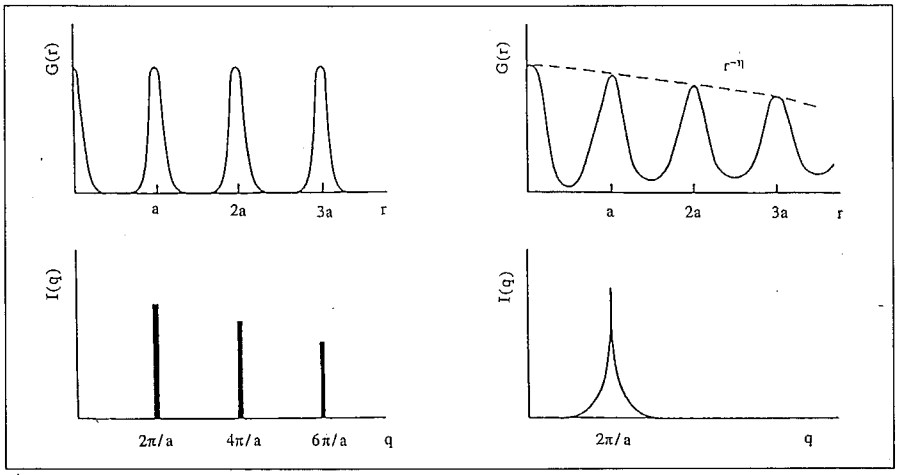

Figure 2. Schematic picture of the pair correlation function G(*r*) and the resulting X-ray intensity *I*(*q*) for (*a*) long range ordering and (*b*) algebraically decaying ordering.

phase transition temperature (T_{AN}), where B approaches zero. At all other temperatures, $\eta \approx 0$, which results in a saturated lineshape with essentially $1/q^2$ tails. This can make the discrimination between Caillé lineshapes and normal Bragg peaks difficult. Nevertheless Caillé lineshapes have been demonstrated for monomeric smectic liquid crystals [3], smectic polymers [4] and surfactant membranes [5].

Conformal and independent fluctuations in freely suspended smectic films

A unique property of smectic liquid crystals is their ability to form films that are freely suspended over an aperture in a frame. In such a film the smectic layers align with a high degree of uniformity parallel to the two flat air-film interfaces. To accomplish X-ray reflectivity measurements–which give a large footprint at small incident angles–we succeeded in making films as large as 1×3 cm^2. Even for such areas the film thickness L can be easily varied from several hundreds of molecular layers (some μm and thus essentially bulk systems) down to two layers (typically 5–6 nm). Because of these properties freely suspended smectic films constitute ideal model systems.

Similarly to rough surfaces the thermal fluctuations of the smectic layers in a film give rise to diffuse scattering at angles away from the specular reflectivity (see Appendix). The intensity depends on the wavelength of the fluctuations and is determined by the layer displacement function $\langle u^2(0,z)\rangle$ and the interlayer displacement-displacement correlation function $C(\mathbf{R},z,z')=\langle u^2(\mathbf{R},z)u^2(0,z')\rangle$. Here $\mathbf{R}$ is in the plane of the film and z along the normal, while the displacement functions depend on the surface tension γ and the elastic constants B and K [6]. At long in-plane length scales $R>R_c$ (small wave vectors) all the layers are found to fluctuate conformally, i.e. they move in unison [7]. For $R>R_c$ such a conformality is expected to vanish (see figure 3), starting between top and bottom of the film. In general, $R_c \approx (L/B)^{1/2}$, hence loss of conformality can be expected at large in-plane wave vectors (small R) for thick films and/or systems with a small value of B.

The liquid crystalline compound *p*,*p*'-diheptylazoxybenzene (7AB) has been used (see figure 4). We worked about 0.5°C below the second-order smectic– nematic phase transition [8], where B can be expected to become small, and with two film thicknesses (24 and 100 layers). The observed intensity is essentially the Fourier transform of $C(\mathbf{R},z,z')$ [6, 7]. Specular scans (along q_z at $q_y = 0$) and diffuse longitudinal scans (along q_z at constant q_y) for a 24 layer film as taken at beamline BM32 at ESRF (Grenoble) are presented in figure 5(*a*). At small q_y the diffuse scattering is the coherent superposition of the scattering from each layer, showing maxima and minima at the same positions as the specular reflectivity. This is the signature of conformality [9]. The disappearance of the interference fringes at large q_y indicates that top and bottom of the film no longer fluctuate in unison. At the same point the broadening and weakening of the Bragg peak reveals that less than the total number of layers contributes coherently to the diffuse signal. The similar slopes of the transverse diffuse scans at the Bragg peak and its subharmonic (figure 5(*b*)) indicate that lateral correlations between adjacent and next nearest layers persist down to molecular length scales. At the same time the very different slope of the scan at $q_z = 0.7q_0$ confirms the absence of conformality between top and bottom of the film. A more quantitative description has been given elsewhere [10].

In conclusion a crossover from conformal fluctuations (at large wavelength) to independent fluctuations (at shorter wavelength) has been observed in freely suspended smectic films. The specific geometry to measure the diffuse scattering in combination with the large dynamic range possible at a third

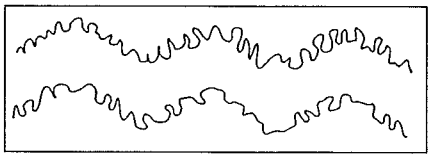

Figure 3. Conformal and independent fluctuations of top and bottom of a smectic film at long and short wavelengths, respectively.

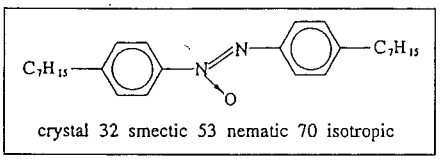

Figure 4. The compound 7AB and its phase transitions (°C).

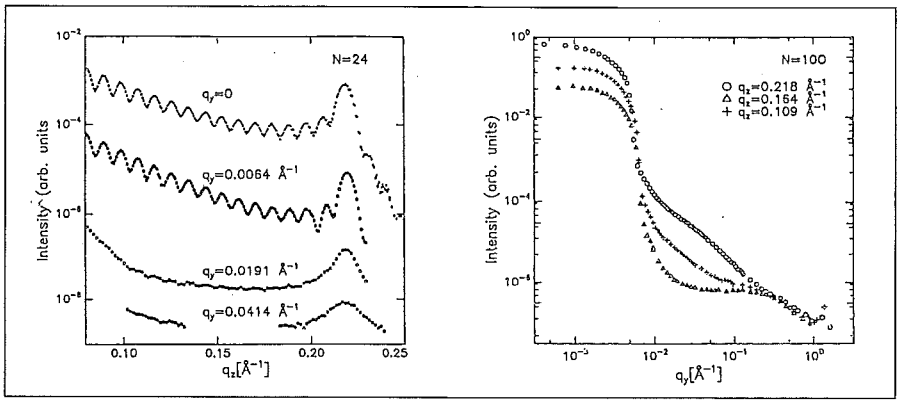

Figure 5. (*a*) Longitudinal diffuse scans of a 24 layer film of 7AB. (*b*) Transverse diffuse scans of a 100 layer film at (from top to bottom) the Bragg peak ($q_z = q_0$), a subharmonic ($q_z = 0.5q_0$), and an intermediate position $q_z = (0.7q_0)$.

generation synchrotron allowed us to probe wave vectors down to inverse lateral distances between molecules.

Induction of true long-range order in smectic elastomers

In a smectic side-chain polymer (figure 1(*b*)) the mesogenic molecules are attached to polymer chains via flexible spacer groups. Although the phase transition temperatures can differ significantly from those of its monomeric counterpart due to the coupling between the '1-D' layers and the ensemble of polymer chains, the Landau–Peierls instability persists in such systems [4]. These liquid crystalline polymers can be weakly crosslinked into an elastomer network (figure 1(*c*) with almost no change in the phase transition temperatures. In such a smectic elastomer, however, the fluctuating smectic layers cannot move past crosslinks in the network. The network coupling imposes a penalty for relative translations between the orientationally ordered fluid layers and the polymer network. A recent continuum theory has predicted that the fluctuations associated with the Landau-Peierls instability can be suppressed in this situation [11]. The marginally stable,quasi-periodic structure of normal '1-D' fluid stacks should be transformed into a fully periodic one with proper long range order, and the resultant diffraction should change from Caillé lineshapes to normal Bragg peaks (see figure 2).

Measurements for both an uncrosslinked smectic acrylate and the corresponding crosslinked polymer [12] (see figure 6) were done at T=55.0°C, which is in the smectic-A phase well below T_{AN} and well above the glass transition T_g. In order to get monodomain samples, the uncrosslinked polymer has been aligned with a magnetic field. In contrast, the liquid crystalline groups in the crosslinked elastomer have been aligned with a strain field, which was applied *in situ* to freely suspended samples. At beamline X-10A (NSLS, Brookhaven National Laboratory, USA.) multiple-Bragg reflections were used for the monochromator and the analyser crystals, leading to a strong fall-off of the intensity of the incident beam according to $1/q^{3.6}$. This is much sharper than $1/q^2$ and therefore sufficiently steep for the present lineshape measurement. To appreciate the situation it is important to realize that a Caillé lineshape cannot have an asymptotic q-dependence that is steeper than $1/q^2$, whereas the behaviour of a true Bragg peak is not bound by this constraint. Even a Bragg peak that has been broadened by lattice imperfections can in principle still be sharper than $1/q^2$ and may not reach this asymptotic limit for several decades of intensity.

Figure 7(*a*) shows the scattering intensity from the first-order diffraction of both the crosslinked elastomer and the corresponding uncrosslinked polymer. Figure 7(*b*) compares the asymptotic slopes of both peaks [13]. The intensity tails of the uncrosslinked polymer have a slope of -1.85±0.10. This value is somewhat less than the theoretical limit of 2 due to the finite mosaic width of the sample [14]. This mosaic width, which measures the variation of layering directions about the average, was 2.5° for the elastomer and 4.1° for the polymer. In fact, the mosaic distribution causes the Caillé lineshape to vary continuously between a power law with an exponent of $2-\eta$ (for a single orientation sample with no mosaic spread) to one with an exponent of $1-\eta$ (for a random powder). Hence any value between the limits 1 and 2 is evidence for a Caillé lineshape. In contrast to the lineshape of the

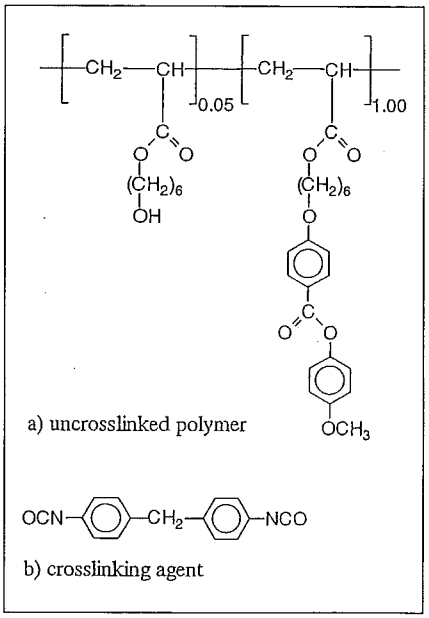

Figure 6. The uncrosslinked side-chain liquid crystalline polymer (M_n = 11,200 g mol^{-1}) has been synthesized by radical copolymerization. It has 5 mol% side chains which terminate with hydroxyl groups and which are crosslinked to obtain the elastomer. The phase transitions for uncrosslinked polymer (g 26 S_A 82 N 110 I) and elastomer (g 31 S_A 80 N 111 I) are very similar.

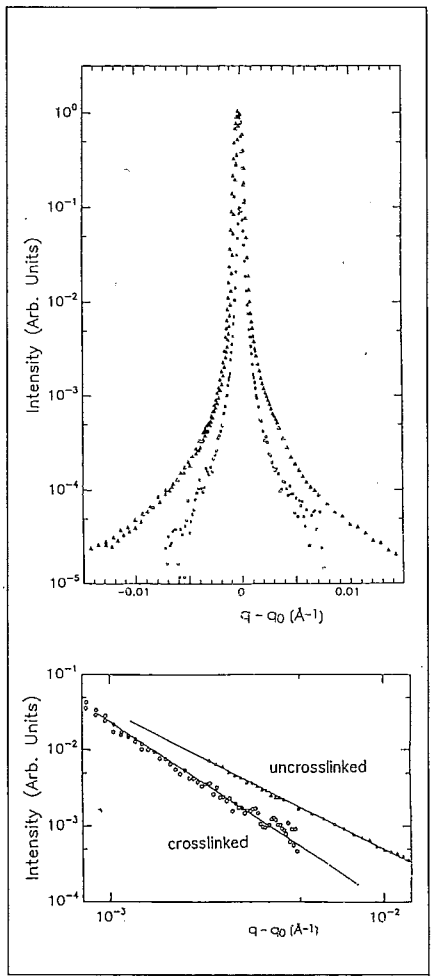

Figure 7. (*a*) First-order diffraction intensity from the smectic uncrosslinked polymer (squares) and elastomer network (triangles), respectively. The polymer data are shifted one decade down for clarity. (*b*) Comparison of the diffraction intensity tails from the elastomer (circles, slope −2.40±0.10) and the corresponding uncrosslinked polymer (triangles, slope −1.85±0.10).

uncrosslinked polymer, the scattering intensity for the smectic elastomer decreases rapidly away from q_0, with a slope of −2.40±0.10 on a log–log plot over 3 orders of magnitude. Hence the Bragg scattering from the elastomer is significantly sharper than a Caillé power-law lineshape, which saturates at a limiting slope of −2. Clearly, the dramatic sharpening of the elastomer lineshape is correlated with the existence of percolating crosslinks and the resultant change in polymer topology.

In summary, we have found the first evidence for the existence of long range translational order in soft '1-D' layered systems embedded in 3-D space, by examining a weakly crosslinked smectic elastomer network [13]. The stability of the layered structure against thermal fluctuations is dramatically enhanced by the crosslinked architecture, to the extent that the usual Landau–Peierls instability and the resultant logarithmically divergent mean squared layer displacements are no longer observed.

Acknowledgements

We would like to thank R. Zentel for valuable discussions and providing us with the polymer and elastomer, J.-M. Petit and F. Rieutord (ESRF), and H. Shao and K. Liang (BNLS) for experimental assistance at the synchrotron experiments. This work is part of the research program of the Stichting voor Fundamenteel Onderzoek der Materie (Foundation for Fundamental Research on Matter (FOM)) and was made possible by financial support from the Nederlandse Organisatie voor Wetenschappelijk Onderzoek (Netherlands Organisation for the Advancement of Research (NWO)).

Appendix: Specular and diffuse X-ray reflectivity

X-ray reflectivity is concerned with an X-ray beam of wavelength λ or wave vector $k = 2\pi/\lambda$ incident under a small angle α on a surface. A typical experimental situation is shown in figure A1, with for $\psi=0$ the wave the vector $\mathbf{k_f}$ of the outgoing beam in the plane of incident wave vector and the surface normal. For elastic scattering $|\mathbf{k_i}| = |\mathbf{k_f}| = |\mathbf{k}|$ and the wave vector transfer is given by $\mathbf{q} = \mathbf{k_f} - \mathbf{k_i} = 2k \sin\alpha$. For specular reflectivity $\alpha = \beta$ and $q = q_z$ parallel to the surface normal. The scattering of such a plane wave can be described in terms of a macroscopic index of refraction n, which (neglecting absorption) can be written as $n \approx 1 - \delta$, with $\delta = \rho_e r_e \lambda^2/2\pi$ where ρe is the electron density of the medium and r_e the classical radius of the electron. For many materials of interest δ is of the order of 10^{-6}, so that n is slightly smaller than 1. Hence according to Snell's law the X-ray beam is refracted away from the normal to the interface and for small angles $\alpha < \alpha_c = \cos^{-1}(n) \approx 0.15°$ total reflection occurs. For $\alpha > \alpha_c$ the specularly reflected intensity R_F is given by Fresnel's law:

$$\mathbf{R_F} = \left| \frac{\sin\alpha - (n^2 - \cos^2\alpha)^{1/2}}{\sin\alpha + (n^2 - \cos^2\alpha)^{1/2}} \right|^2 \approx \left(\frac{\alpha_c}{2\alpha} \right)^4,$$

where the last approximate equality holds for $\alpha >> \alpha_c$. A typical reflectivity curve showing these features is given in figure A2(*a*).

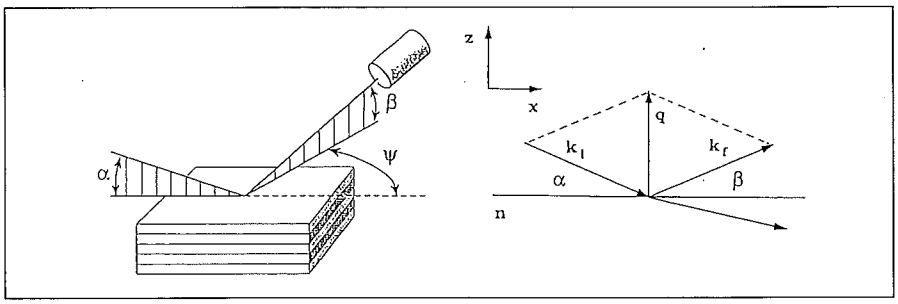

Figure A1. Scattering geometry in (*a*) real space and (*b*) reciprocal space for $\alpha = \beta$ and $\psi = 0$.

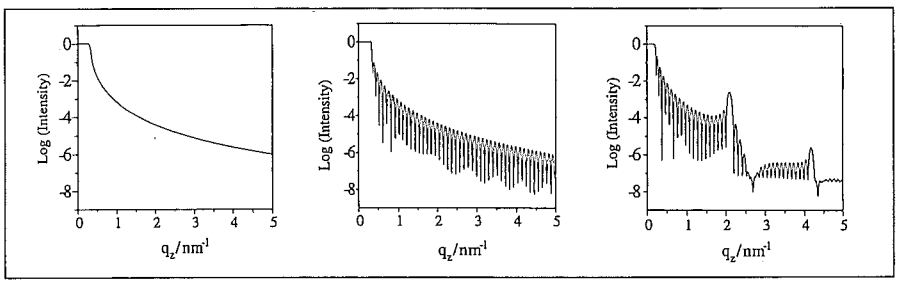

Figure A2. Model calculations of (*a*) Fresnel reflectivity of a single interface ($\delta = 4\times10^{-6}$), (*b*) reflectivity of a 60 nm isotropic film ($\delta = 4\times10^{-6}$), and (c) the same film with an internal periodic structure of 3 nm with $\delta_1 = 4\times10^{-6}$ (1.6 nm central part smectic layers) and $\delta_2 = 2\times10^{-6}$ (0.7 nm outer parts smectic layers).

Without going into further details we remark that in the case of an isotropic structureless film, reflection also occurs at the second interface. Interference between the two reflected signals – that have acquired a phase difference proportional to the film thickness – leads to interferences (Kiessig fringes) on top of the Fresnel reflectivity (see figure A2(*b*)). Finally in the case of a freely suspended smectic film the periodic layer structure gives rise to finite size broadened Bragg-like peaks, that in turn are superimposed on this structure (see figure A2(*c*)). Hence

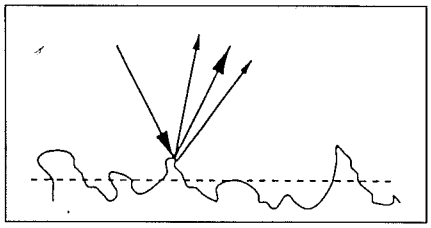

Figure A3. Microscopic roughness or fluctuations leading to a diffuse component of the reflectivity.

specular X-ray reflectivity measurements can be interpreted as the result of these various effects, with the average electron density profile along the film normal as an important parameter. In addition roughness or fluctuation effects have to be taken into account.

Figure A3 shows roughness c.q. fluctuations on a microscopic scale which causes scattering away from the specular condition. The resulting diffuse reflectivity can be measured by rocking the film so that $\alpha+\beta=$ constant with $\alpha \neq \beta$ at $\psi=0$ (q_x scan, see figure A1). As smectic A systems are uniaxial alternatively the detector can be moved out of the scattering plane over an angle ψ (q_y scan, see figure 5(*b*)). In figure 5(*a*) the wavelength dependence of the fluctuations is probed by making q_z scans ($\alpha = \beta$, parallel to the specular direction) at various offsets of ψ setting q_y.

References

1. See, for example, CHAIN, P. M., and LUBENSKY, T. C., 1995, *Principles of Condensed Matter Physics* (New York: Cambridge University Press).
2. CAILLÉ, A., 1972, C. R. Acad. Sci. Paris **B 274**, 891.
3. ALS-NIELSEN, J., LISTER, J.D., BIRGENEAU, R.J., KAPLAN, M, SAFINYA, C.R., LINDEGAARD-ANDERSEN, A., and MATHIESEN, S., 1980, *Phys. Rev.* B, **22**, 312.
4. NACHALIEL, E., KELLER, E. N., DAVIDOV, D., and BOEFFEL, C., 1991, Phys. Rev. A, 43, 2897.
5. SAFINYA, C. R., ROUX, D., SMITH, G. S., SINHA, S. K., DIMON, P., CLARK, N. A., and BELLOCQ, A. M., 1986, *Phys. Rev.* Lett., **57**, 2718.
6. HOLYST, R., 1991, *Phys. Rev.* A, **44**, 3692; SHALAGINOV, A. N., and ROMANOV, V. P., 1993, *Phys.Rev.* E, **48**, 1073.
7. MOL, E. A. L., SHINDLER, J. D., SHALAGINOV, A. N., and DE JEU, W. H., 1996, *Phys. Rev.* E, **54**, 536.
8. GRAMSBERGEN, E. F. and DE JEU, W. H., 1988, *J. chem. Soc. Faraday Trans.* 2, **84**, 1015.
9. SINHA, S. K., 1991, *Physica* B, **173**, 25.
10. MOL, E. A. L., WONG, G. C. L., PETIT, J.-M., RIEUTORD, F., and DE JEU, W. H., 1997, *Phys. Rev. Lett.*,**79**, 3439.
11. TERENTJEV, E. M., WARNER, M., and LUBENSKY, T. C., 1995, *Europhys. Lett.*, **30**, 343.
12. ZENTEL, R., and BENALIA, M., 1987, *Makromol. Chem.*, **188**, 665.
13. WONG, G. C. L., DE JEU, W. H., SHAO, H., LIANG, K. S., and ZENTEL, R., 1997, *Nature*, **389**, 576.
14. KAGANER, V. M., OSTROVSKII, B. I., and DE JEU, W. H., 1991, *Phys. Rev.* A, **44**, 8158.